ELSEVIER

Journal of Structural Geology 25 (2003) 2089–2107

JOURNAL OF STRUCTURAL GEOLOGY

www.elsevier.com/locate/jsg

Microstructural evolution of the Seridó Belt, NE-Brazil: the effect of two tectonic events on development of *c*-axis preferred orientation in quartz

Mário Neto Cavalcanti de Araújo[a,b,*], Fernando César Alves da Silva[b], Emanuel Ferraz Jardim de Sá[b], Rodney J. Holcombe[c], Paulo Marcos de Vasconcelos[c]

[a]*Departamento Geologia e Recursos Naturais, Instituto de Geociências, Universidade Estadual de Campinas, P.O. Box 6152, Campinas, SP 13083-970, Brazil*
[b]*Pós-Graduação em Geodinâmica e Geofísica, Universidade Federal do Rio Grande do Norte, Nata, RN-Brazil*
[c]*Department of Earth Sciences, The University of Queensland/Brisbane, Queensland, 4072, Australia*

Received 28 November 2001; received in revised form 20 March 2003; accepted 24 March 2003

Abstract

The polyphase evolution of the Seridó Belt (NE-Brazil) includes D_1 crust formation at 2.3–2.1 Ga, D_2 thrust tectonics at 1.9 Ga and crustal reworking by D_3 strike-slip shear zones at 600 Ma. Microstructural investigations within mylonites associated with D_2 and D_3 events were used to constrain the tectono-thermal evolution of the belt. D_2 shear zones commenced at deeper crustal levels and high amphibolite facies conditions (600–650 °C) through grain boundary migration, subgrain rotation and operation of quartz $\langle c \rangle$-prism slip. Continued shearing and exhumation of the terrain forced the re-equilibration of high-T fabrics and the switching of slip systems from $\langle c \rangle$-prism to positive and negative $\langle a \rangle$-rhombs. During D_3, enhancement of ductility by dissipation of heat that came from syn-D_3 granites developed wide belts of amphibolite facies mylonites. Continued shearing, uplift and cooling of the region induced D_3 shear zones to act in ductile-brittle regimes, marked by fracturing and development of thinner belts of greenschist facies mylonites. During this event, switching from $\langle a \rangle$-prism to $\langle a \rangle$-basal slip indicates a thermal path from 600 to 350 °C. Therefore, microstructures and quartz *c*-axis fabrics in polydeformed rocks from the Seridó Belt preserve the record of two major events, which includes contrasting deformation mechanisms and thermal paths.

Keywords: Microstructures; Deformation mechanisms; Mylonites; Quartz *c*-axis fabrics

1. Introduction

The tectonothermal evolution of polydeformed terrains encompasses production of several sets of structures, superimposed kinematics, overprinting of metamorphic assemblages and multiple magmatic pulses. The interplay of these processes during superimposed deformational events results in transposition or complete erasing of previous structures and mineral assemblages, hampering the investigation of thermal conditions associated with the early events. In many instances, the scarcity of mineral assemblages owing to either compositional matters or obliteration by subsequent events contributes to the absence of records of the first thermal episodes. In this case, interpretation of the tectonothermal evolution using only the analysis of mineral assemblages and geometry of structures within mylonite zones and surrounding rocks is not simple. In such a scenario, microstructures and quartz *c*-axis fabrics in quartz can provide significant information on thermal conditions for three main reasons: (i) it is a common mineral in the majority of the crustal rocks, (ii) it occurs in a large range of metamorphic conditions and (iii) it displays a variety of temperature dependent deformation textures that can be investigated by conventional petrography.

Although many researches have focused on the modification of microstructures and *c*-axis fabrics in quartz during superposed tectonothermal events (Jessel and Lister, 1990; Gleason et al., 1993), some have tried to investigate the extent to which *c*-axis fabrics are preserved during overprinting events (White and Mawer, 1992; Ralser, 2000). This is the main scope of the present paper, which focuses mainly on the preservation and significance of microstructures and quartz *c*-axis fabrics in a polydeformed terrain from the northeast

* Corresponding author.
E-mail address: mariogeo@ige.unicamp.br (M.N. Cavalcanti de Araújo).

0191-8141/03/$ - see front matter © 2003 Elsevier Ltd. All rights reserved.
doi:10.1016/S0191-8141(03)00069-5

Borborema Province (the Seridó Belt; Fig. 1). It is worth mentioning that the generation of the Borborema Province during de Brasiliano-Pan African orogeny (600 Ma) involved the assemblage of several terrains, which includes gneissic blocks with Paleoproterozoic ages, minor Archean Nuclei and supracrustal sequences that vary in age from Paleo- to Neoproterozoic.

During the last decades many arguments have been raised on the significance and timing of older subhorizontal foliations marked in augen gneisses and supracrustal rocks

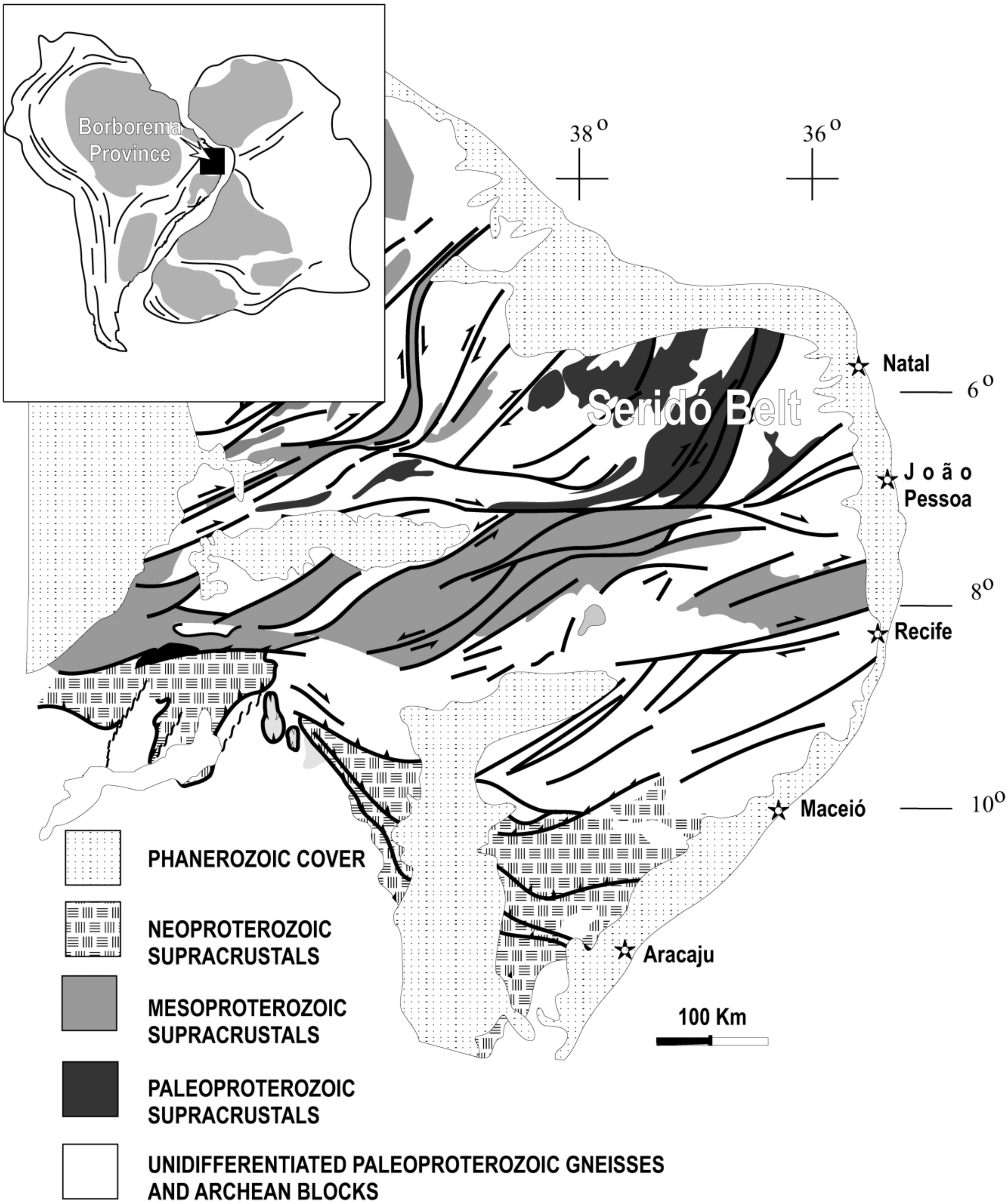

Fig. 1. Location of the Seridó Belt and main tihotectonic domains of the Borborema Province, northeastern Brazil.

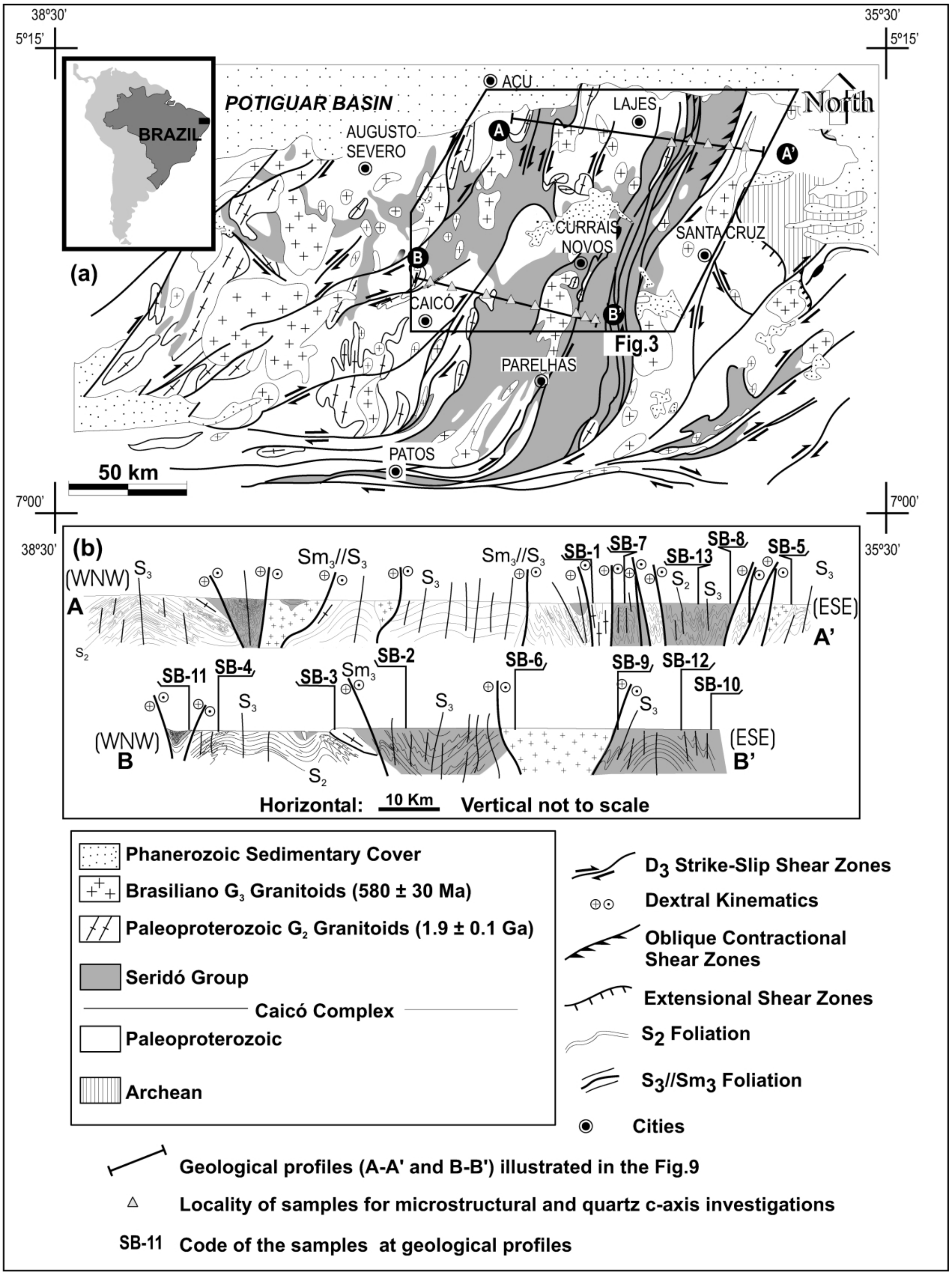

Fig. 2. (a) Geological map of the Seridó Belt with the major lithologic divisions. Inset indicates studied area. (b) Lithostructural profiles (A–A′ and B–B′) across the main trend of the belt. Samples for microstructural analysis are shown as gray triangles in (a) and numbers in (b).

from the Borborema Province and correlatives belts in Africa such as the Trans-Saharan Belt (see Affaton et al., 1991; Boullier, 1991). Jardim de Sá et al. (1995) and Bertrand and Jardim de Sá (1990) state that parts of these structures are ascribed to the 2.0 Ga Transamazonian/Eburnean orogeny. In contrast, Caby et al. (1995) and Archanjo and Bouchez (1991) argue for a Neoproterozoic age (600 Ma) for all ductile fabrics present in the northeast segment of the Borborema Province. New geochornological U–Pb and Sm–Nd data (Kozuch et al., 1997) suggest a polycyclic evolution for the belts of this portion of the region; nevertheless, structural similarities with flat-lying structures from Neoproterozoic parts of Borborema Province (Neves et al., 2000) demonstrate the necessity of more work on this theme. Distinction between tectonothermal regimes with a basis on *c*-axis fabrics in quartz associated with the Transamazonian and Brasiliano deformational fabrics in the Seridó Belt adds constraints on the current debate of superimposed events in the region. To do so, a set of microscopic deformation fabrics and quartz *c*-axis fabrics are used to address how microstructures and crystallographic preferred orientation preserve the record of the polyphase evolution of the belt.

2. Geological setting

The Seridó Belt (Fig. 2) encompasses a paleoproterozoic basement (Caicó Complex), a younger supracrustal sequence (Seridó Group), and two generations of granitoids. The Caicó Complex includes Paleoproterozoic granite-gneisses, with minor remnants of metasediments and amphibolites. In its easternmost portion, the Caicó Complex includes a 3.1–3.4 Ga Archean block, which is made up mainly of migmatites and anatectic gneiss complexes. The supracrustal sequence (Seridó Group) comprises a basal formation (Jucurutu Fm.) of paragneiss, calc-silicate rocks and marble; an intermediate formation (Equador Fm.) of quartzite and metaconglomerate, and an upper formation (Seridó Fm.) represented by aluminous to feldsphatic mica schists.

The evolution of the Seridó Belt includes crust formation at 2.3–2.1 Ga, metamorphism at 2.0 ± 0.05 Ga (Dantas et al., 1999) and intrusion of syn to late tectonic granites at 1.9 Ga coeval with the Transamazonian/Eburnean orogeny, followed by the Pan-African/Brasiliano event associated with the assemblage of the Western Gondwana at 600 Ma. The former is principally an event of crustal reworking of Paleoproterozoic fabrics by NE-trending strike-slip shear zones and intrusion of syntectonic plutons dated at 580 ± 30 Ma (Rb–Sr whole-rock isochrons, U–Pb zircon ages;Leterrier et al., 1994). Late-Brasiliano ductile-brittle to brittle deformation, cooling and post-tectonic plutonism, as suggested by Rb–Sr, K–Ar and $^{40}Ar–^{39}Ar$ ages, occurred at 540 and 500 Ma (Corsini et al., 1998).

The main question concerning the tectono-metamorphic evolution of the Seridó Belt is whether or not the Transamazonian event affected its whole stratigraphic sequence. Caby et al. (1995) advocate that the Transamazonian orogeny appears only in the basement unit, referred to as the Caicó Complex, whereas the upper unity of the belt (the Seridó Group) has experienced solely the Brasiliano deformation. Such interpretation is supported by recent SHRIMP U†Pb ages in the range of 1000–640 Ma obtained on detrital zircons of the upper Seridó Group (Van Schmus et al., 2000), which may have been deposited as flysch basins upon the Trasamazonian basement during the Brasiliano orogeny. Even with this data, the interpretation of the tectono-thermal evolution of the Seridó Belt remains controversial. A great amount of evidence documents the presence in the Seridó Group of ductile fabrics that match the metamorphic grade, tectonic framework and kinematics of those related to the Transamazonian fabrics within the basement rocks. This evidence is summarized in the work of Jardim de Sá et al. (1995), in which they state that the Seridó Group experienced conflicting metamorphic grades, incompatible kinematic events and 1.9 Ga granitic magmatism.

3. Tectonic evolution

The structural framework of the Seridó Belt consists of three main deformation phases, D_1, D_2 and D_3. The oldest deformation event (D_1) produced a migmatitic-gneissic layering (S_1), restricted to the basement unit and variably affected by the subsequent D_2 and D_3 events. During the D_2 event, the S_1 gneissic layering of the Caicó Complex as well as the S_0 bedding of metasediments from the Seridó Group were folded into F_2 isoclinal recumbent folds to produce the S_2 flat-lying foliation. This event is associated with the development of low-angle shear zones, S–SE verging nappes and the syntectonic emplacement of the 1.9 Ga granitoids. Sillimanite, garnet, kyanite, staurolite and ductilely deformed feldspar aligned in S_2 indicate that the D_2 event occurred under intermediate pressures (>6 kbars) and at temperatures higher than 600 °C (Fonseca et al., 1991). Such characteristics combined with the observation of lithostratigraphic inversions defined by the local presence of allochthonous slices of the Caicó Complex overlying the Seridó Group, suggest that the D_2 event was associated with thrusting.

The third deformational event (D_3) generated kilometer-scale F_3 synforms and antiforms, with fold axis parallel to NNE-trending D_3 strike-slip shear zones. Although the F_3 folds have subhorizontal hinges and steep axial planes (S_3), their geometry depends on the magnitude of the D_3 strain (Fig. 2b). The F_3 folds are gentle to open in low-strain domains, whereas under high D_3-strain they change from tight to isoclinal. Such strain partitioning is demonstrated by changes of structural styles along the belt. In its central portion, a dextral transpressive regime dominates (Archanjo and Bouchez, 1991; Vauchez et al., 1995), whereas in its

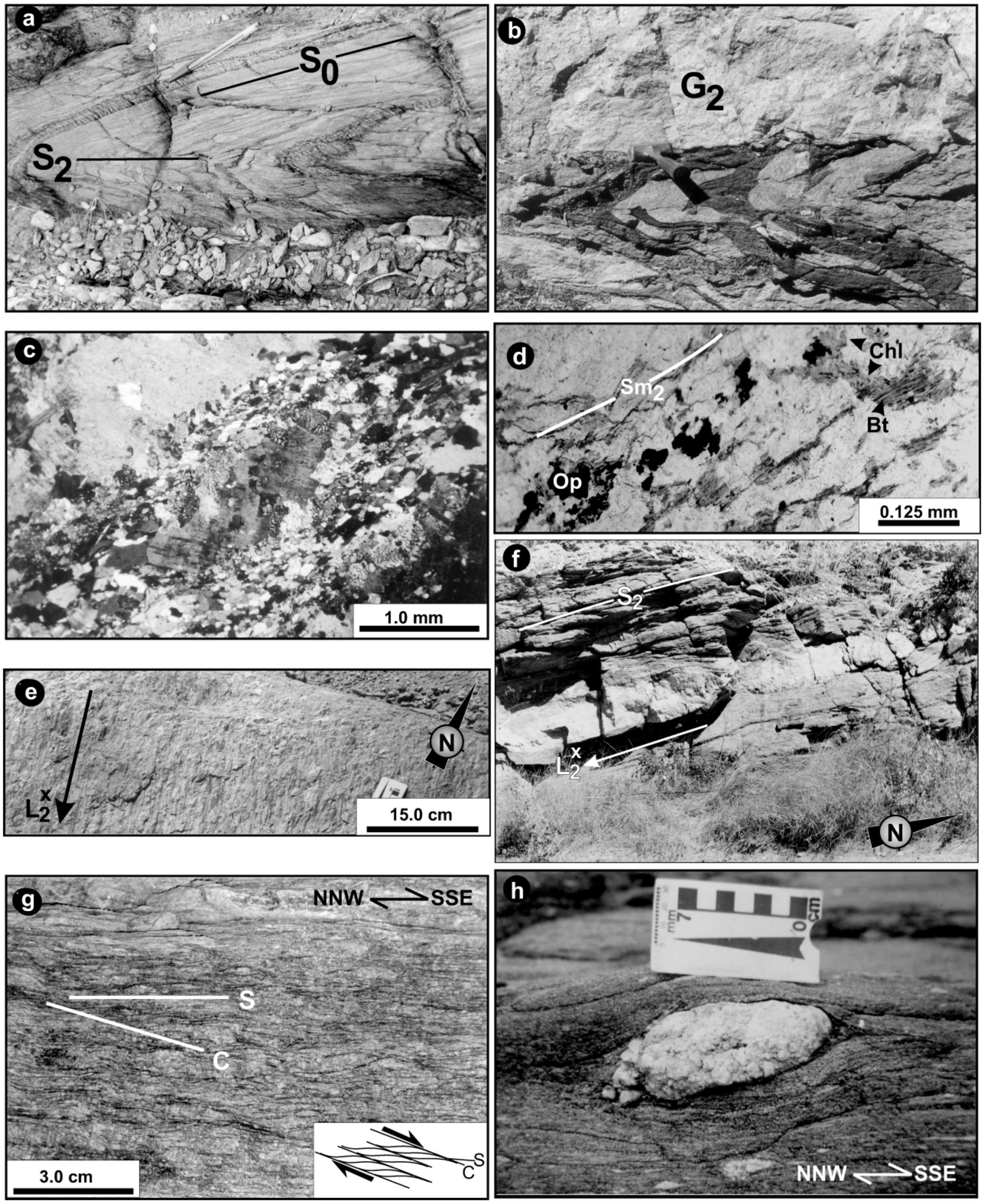

Fig. 3. (a) F_2 recumbent fold affecting the S_0 layering of micaschists from the Seridó Group. (b) F_2 recumbent fold with syn-D_2 metapegmatites emplaced parallel to the axial planar S_2 of a migmatite gneiss from the Caicó Complex. (c) Feldspar porphyroclast rimmed by myrmekite within a syn-D_2 granitoid. (d) Greenschist facies retrogression of biotite (Bt) into chlorite (Chl) + opaque minerals (Op) following the Sm_2 mylonite fabric of micaschist from the Seridó Group. (e) N–S down-dip L_2^x lineation marked by stretched K-feldspar and quartz of a syn-D_2 augen gneiss that intrudes micaschists from the Seridó Group. (f) Boudinaged pegmatite dyke emplaced along the Sm_2 foliation of granite gneiss from the Caicó Complex. The major extension of the boudinage is parallel to the L_2^x stretching lineation indicated by the arrow at the bottom of the figure. (g,h) D_2 SSE-directed transport. (g) S–C structure within a syn-D_2 granitoid emplaced along the Sm_2 fabric of micaschists of the Seridó Group. (h) Asymmetrical tails around pebbles of conglomerates from the Seridó Group.

eastern and western portions, deformation develops in an extensional/transtensional style (Jardim de Sá et al., 1999). Amphibolite facies conditions (600 °C and 3.5 kbars) dominate regionally and are clearly identified in the metapelites from the Seridó Group (Souza, 1996), in which the frequently well-developed S_3 surface contains biotite, muscovite, staurolite, sillimanite, cordierite and garnet with or without andalusite. Retrogressive stages to mid- and low-greenschist conditions are shown by the replacement of the amphibolite facies assemblages by chlorite and muscovite.

The similarity of metamorphic grade between D_2 and D_3 events has been used as an argument against the hypothesis of polyphase evolution of the Seridó Belt. However, textural relationships between mineral paragenesis suggest that the D_2 and D_3 mineral assemblages did not form in a simple progressive P–T path (Fonseca et al., 1991). D_3 metamorphism developed through an anticlockwise trajectory defined by progressive mineral transformations of andalusite into cordierite, sillimanite, followed by a retrogressive stage with the development of chlorite and muscovite (Jardim de Sá et al., 1995). Overprinting of this event on mineral assemblages associated with D_2 is defined by inclusions of kyanite showing transformations into sillimanite and subsequently to muscovite within syn-D_3 andalusite porphyroblasts (Legrand and França, 1989).

4. Structural relationships

The structural elements (folds, foliations, lineations and kinematic indicators), and their relative timing relationships are defined based on field investigations and petrographic data. Special attention will be given to D_2 and D_3 events, which are related to the Transamazonian and Brasiliano orogenies, respectively. It should be noted that D_2 and D_3 events affect a crustal block deformed in a previous event, here referred to as D_1. However, the pervasive overprinting

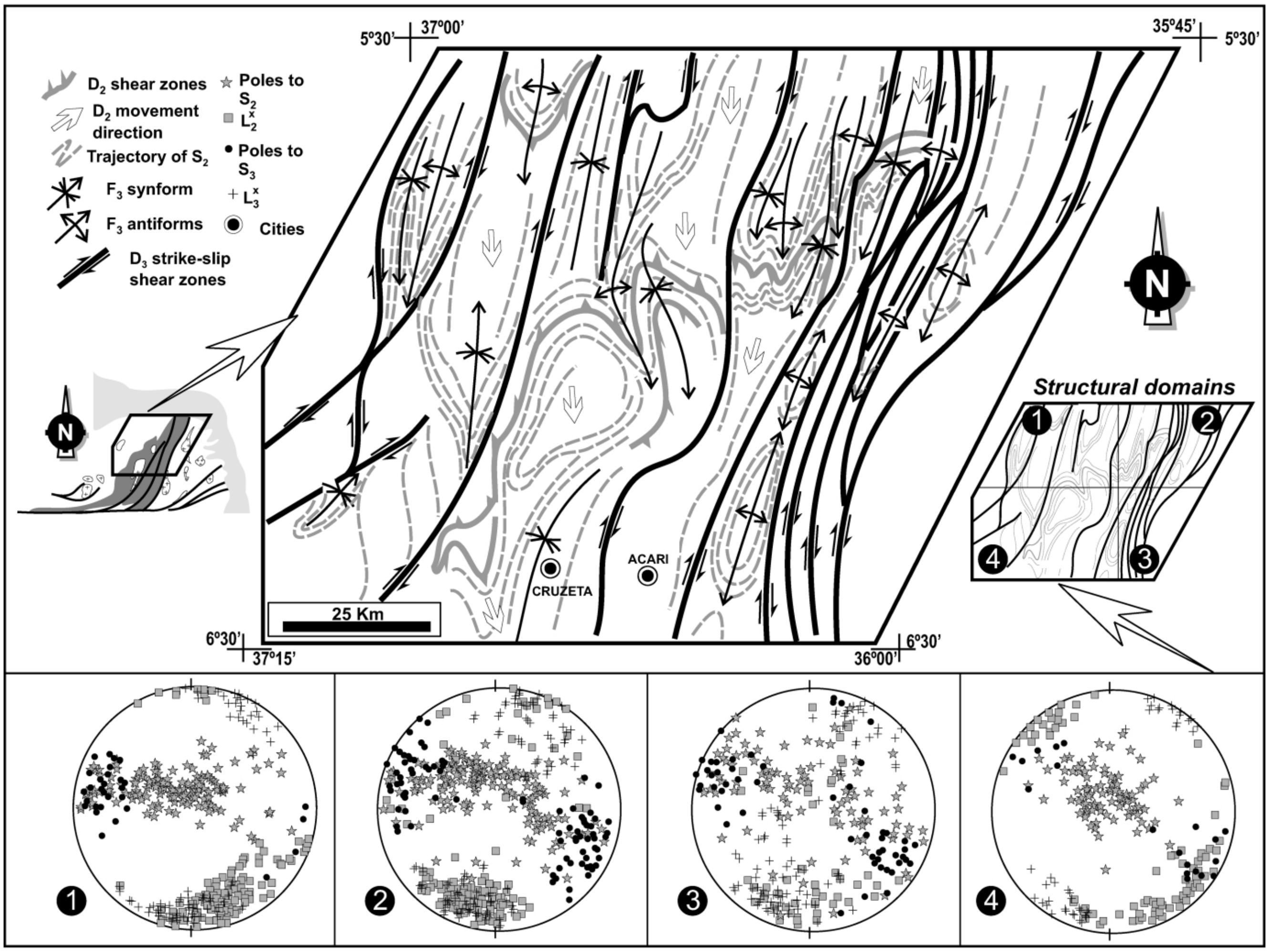

Fig. 4. Structural map of the studied area. It shows trajectory of the S_2//Sm_2 foliation, geometry of D_3 shear zones and the main trend of the F_3 folds. The movement direction of the D_2 tectonics is illustrated by the white arrows, whereas the dextral kinematics along D_3 shear zones is indicated by the black ones. Stereoplots demonstrate the domainal behavior of lineations (L_2^x and L_3^x) and foliations (S_2 and S_3) within the four structural domains shown in the small sketch at the right side of the illustration.

of the subsequent events (D_2 and D_3) on the D_1 fabrics prevents the complete identification of its structural elements. Investigations along low strain pods of gneisses from the Caicó Complex permit us to describe the S_1 fabric in terms of a subhorizontal gently east- or west-dipping gneissic foliation that frequently evolves to a migmatitic layering.

4.1. D_2 event

During D_2, the S_1 foliation of rocks from the Caicó Complex and the S_0 compositional layering of metasediments from the Seridó Group (Fig. 3a), were folded into tight isoclinal recumbent F_2 folds with gentle NW–SE to N–S plunges. These folds commonly develop a well-marked subhorizontal axial planar S_2 foliation that becomes subparallel with S_1 and S_0 surfaces as a result of strain during D_2. Sheets of syn-D_2 microgranites and metapegmatites, emplaced both in the Caicó Complex and Seridó Group, intrude along the axial plane of the F_2 folds (Fig. 3b) and display a strongly penetrative high temperature fabric that is consistent with the S_2 foliation of the host rock (Jardim de Sá et al., 1995). Profound reduction of grain size and intensification of the S_2 foliation towards the D_2 low-angle shear zones defines the Sm_2 mylonitic fabric. High temperatures of mylonitization are demonstrated by recrystallized K-feldspar porphyroclast with core-and-mantle structures or rimmed by myrmekite (Fig. 3c). The development of these structures is consistent with deformation at ≈500 °C (Passchier and Trouw, 1996). The local occurrence of synkinematic garnet porphyroblast wrapped by the Sm_2 mylonitic foliation demonstrates that these temperatures were even higher, reaching upper amphibolite facies conditions (550–650 °C; Mazurek, 1992). Development of D_2 mylonites under temperatures ranging from 500 to 650 °C is interpreted in this paper as being representative of thermal peak conditions during the event of shearing. Likewise, transformation of biotite and feldspar to phyllosilicates, particularly chlorite and muscovite (Fig. 3d), is interpreted as resulting from low-temperature conditions

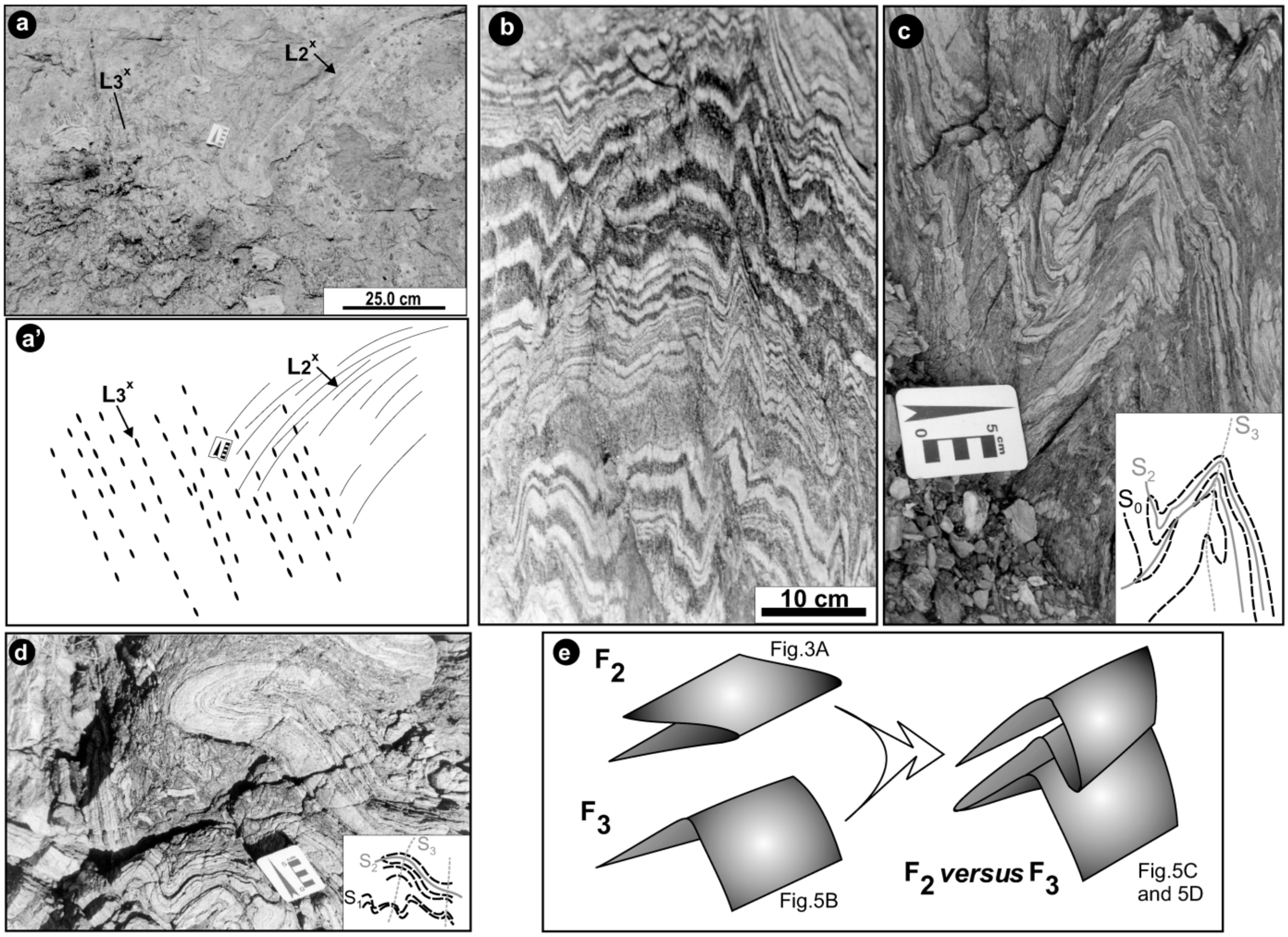

Fig. 5. (a,a′) Plan view of the chronological relationship between L_2^x and L_3^x stretching lineations in micaschists from the Seridó Group. Note that L_2^x, which is marked by quartz rods, is rotated as a result of the D_3 overprinting. (a′) Truncation of L_2^x by L_3^x. (b) F_3 upright fold deforming the $S_0//S_2$ foliation of micaschists. The S_3 foliation forms a well-developed crenulation cleavage that truncates $S_0//S_2$. (c,d) Coaxial fold interference patterns in (c) Micaschists from the Seridó Group, and in (d) migmatite gneiss from the Caicó Complex. (e) Cartoon summarizing the development of the interference patterns by the overprinting of open to gentle upright F_3 folds on the F_2 isoclinal recumbent folds.

(400–450 °C; Yardley, 1989) during the later stages of the D_2 event.

The Sm_2 mylonitic foliation is similarly oriented to the axial planar of F_2 folds, and contains a well-marked N–S down-dip L_2^x stretching lineation (Fig. 3e). This lineation is defined by stretched K-feldspar, quartz and hornblende, in the syn-D_2 granitoids and gneiss from the Caicó Complex, and boudinaged quartz veins, elongated cordierite, kyanite, staurolite and sillimanite porphyroblasts in the metasediments from the Seridó Group. Boudinage of metapegmatite dykes with maximum extension parallel to L_2^x confirms this lineation as a true stretching lineation (Fig. 3f). Southward directed transport along D_2 shear zones is demonstrated by asymmetric F_2 folds with associated NNW–SSE and NNE–SSW trending L_2^x stretching lineation, rotated clasts, asymmetric boudins, S–C structures (Fig. 3g), asymmetric tails around microcline of granite gneiss and pebbles in conglomerates (Fig. 3h).

The S_2, Sm_2 and L_2^x fabrics show a domainal behavior (Fig. 4) with S_2 dipping moderately to west and east due to the superposition of the D_3 event. In some places this foliation is completely rotated and becomes parallel to S_3 (Fig. 4, domains 2 and 3). In Fig. 3 the L_2^x lineation is mostly subhorizontal, however, its orientation deviates from NW–SE in domains 1 and 4 to NE–SW in domains 2 and 3. This is likely to have resulted from the overprinting of the NE-trending D_3 strike-slip shear zones. Rotation of L_2^x during overprinting of the D_3 event is also reproduced in an outcrop-scale, as illustrated in Fig. 5a.

4.2. D_3 event

The D_3 event appears as a complex system of NNE-trending dextral strike-slip shear zones with flanking domains of open to tight NNE-trending F_3 upright folds (profiles A–A′ and B–B′ in Figs. 2 and 5b). The local steeping and refolding of D_1 and D_2 fabrics reveals the effect of D_3 shear zones on the early fabrics. This overprinting produces numerous interference patterns (see Fig. 5c–e), such as types I, II and III of Ramsay and Hubber (1987). The most conspicuous characteristic of the D_3 event is the coexistence of high- and low-temperature mylonitic belts derived from distinct protoliths: metasediments of the Seridó belt, gneisses of the

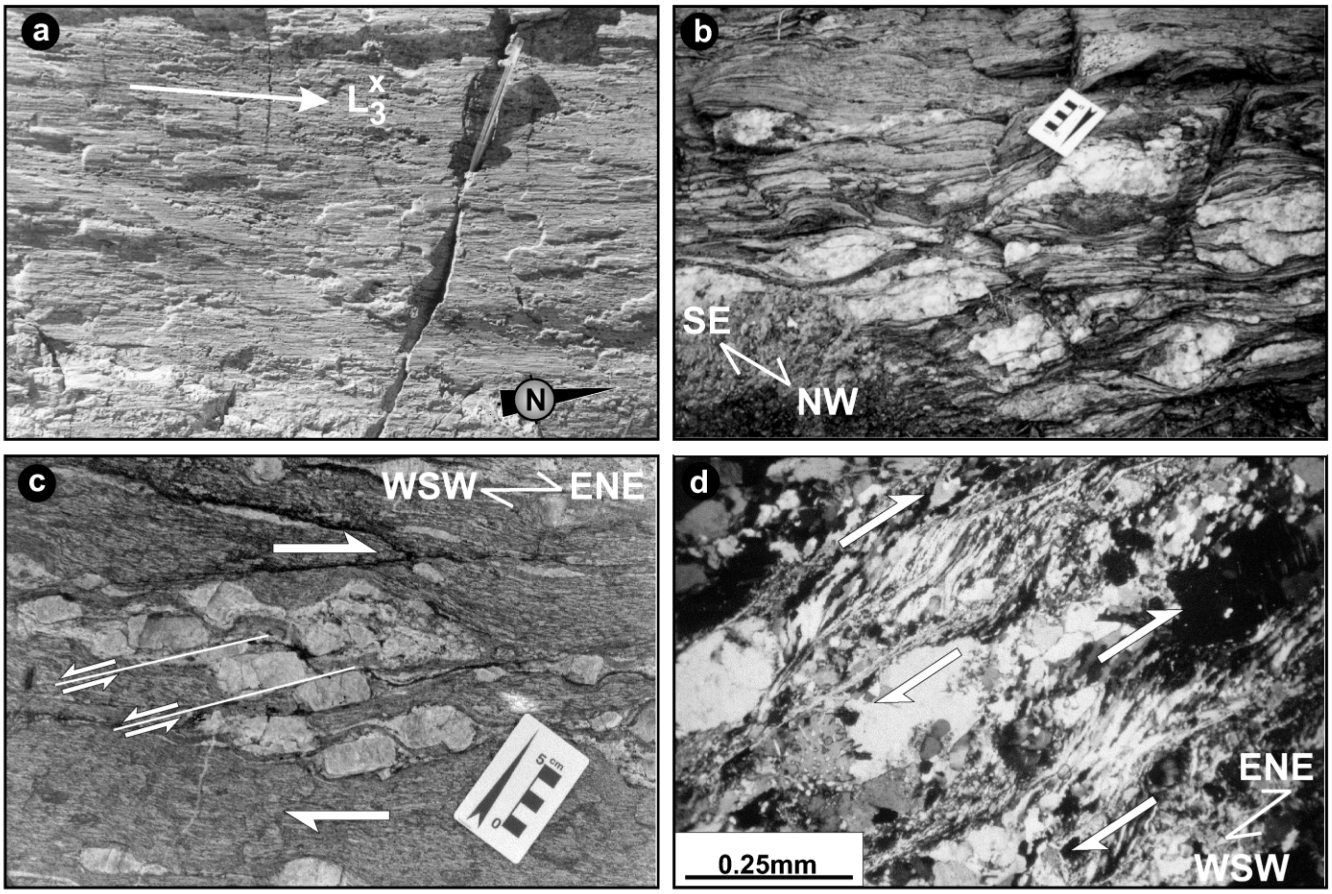

Fig. 6. (a) Field aspect of the L_3^x stretching lineation defined by quartz rods along the S_3 foliation of quartzites of the Seridó Group. (b–f) main kinematic indicators of the D_3 dextral shearing. (b) Asymmetric boudins of quartz within micaschist of the Seridó Group. (c) Mesoscopic dextral shear zone affecting the S_2 gneissic foliation within a granite-gneiss from the Caicó Complex. (d) C′ shear bands indicating dextral sense of shearing. Syn-D_3 granitoid. (e) Tiling of alkali feldspar porphyroclasts. Domino-like structure produced by antithetic shear concentrated along the interface between different porphyroclasts. (f) Dextral micro-shear bands within mylonitic syn-D_3 granitoid.

Caicó Complex and syn-kinematic granitoids. These mylonites usually display a steep-dipping mylonitic foliation (Sm_3) and contain a NNE-trending subhorizontal L2*x* stretching lineation (Figs. 4 and 6a). This lineation is marked by elongated biotite, muscovite, cordierite, andalusite and sillimanite. Transition from high- to low-angle mylonitic zones, consistently bearing a sub-horizontal lineation is locally observed in the south of the Seridó Belt (Fig. 4, domain 3), in which the mylonitic foliation (Sm_3) displays a fan-like geometry, reusing the S_2 foliation as previous heterogeneity (Araújo et al., 2001). In these places, asymmetric tails in syn-D_3 cordierite, sigmoidal quartz veins and shear bands indicate a northward-directed transport that contrasts with D_2 top-to-the-south kinematics. D_3 retrogressive mylonites demonstrated by the replacement of the high-T

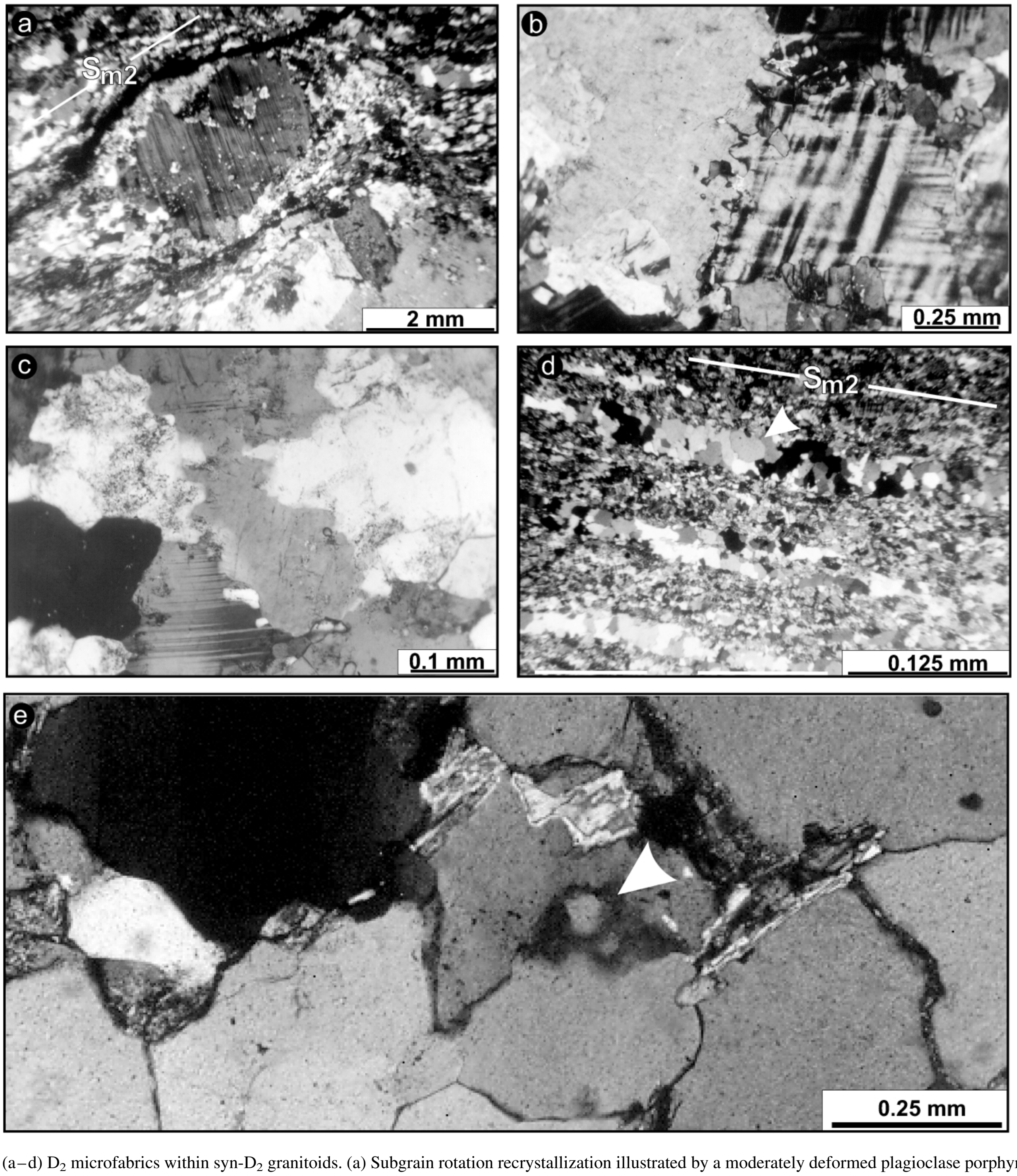

Fig. 7. (a–d) D_2 microfabrics within syn-D_2 granitoids. (a) Subgrain rotation recrystallization illustrated by a moderately deformed plagioclase porphyroclast that is surrounded by a narrow, partial to complete mantle of equant grains. (b) and (c) Amoeboid contacts of alkali feldspars and plagioclases indicating grain boundary migration recrystallisation. Outcrop of G_2 granitoid located approximately 60 km SW of Angicos city. (d) Straight polycrystalline quartz ribbons following the Sm_2 mylonitic fabric. (e) Bulging structure in quartz grain of micaschist from the Seridó Group.

mineral assemblages for chlorite and muscovite develops within or at the boundaries of the high-T mylonitic belts. This suggests further localization of deformation with decreasing temperature, which is likely to be associated with heat dissipation during the cooling of the syn-D_3 granitoids.

The dextral shear sense along D_3 strike-slip shear zones is demonstrated by asymmetric tails in microcline and plagioclase, pressure shadows in garnet, cordierite and andalusite; σ- and δ-type porphyroclasts, asymmetric boudinage, shear bands, S–C and C′ structures, and mica fishes (Fig. 6b–d).

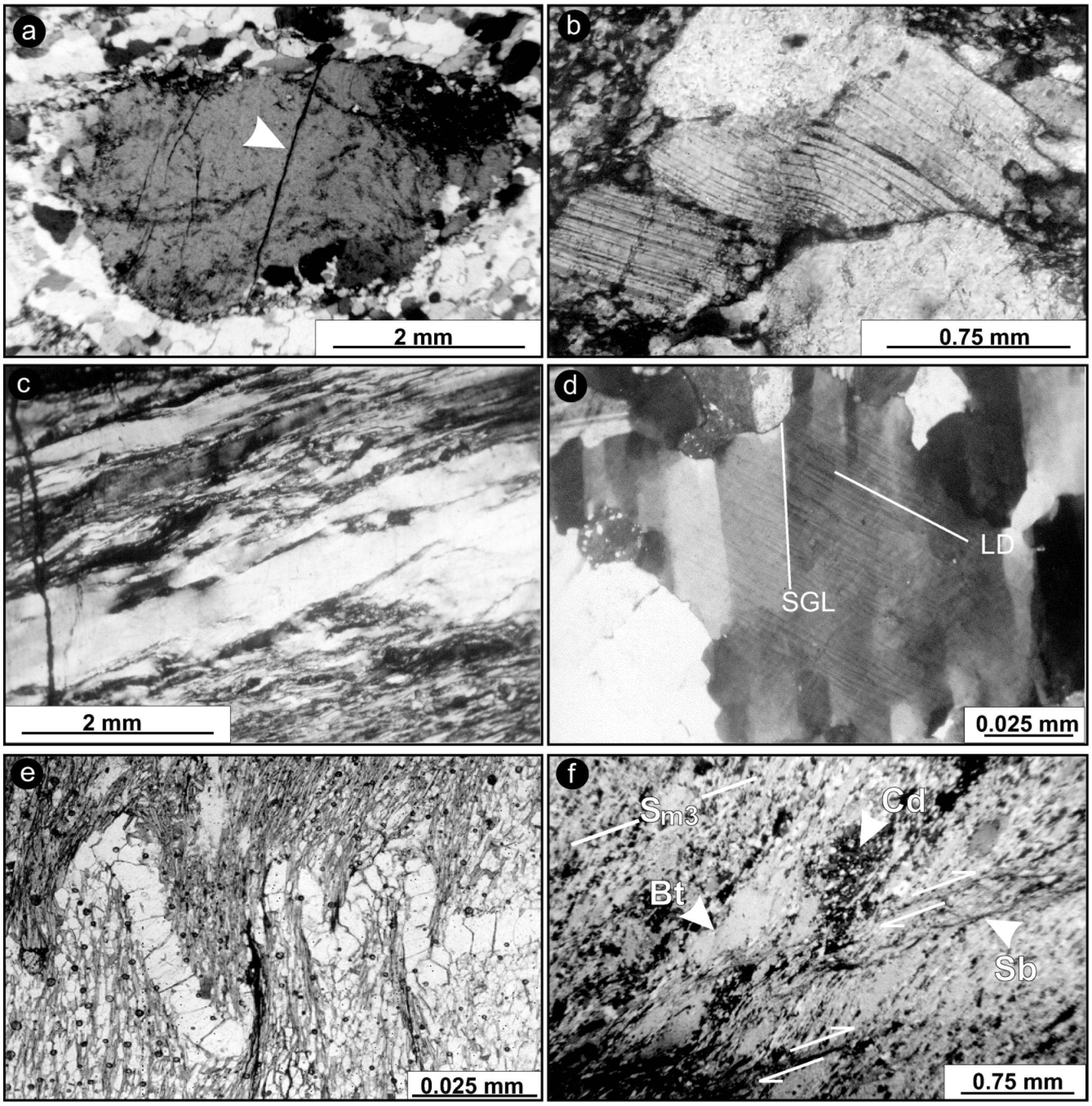

Fig. 8. D_3 microfabrics. (a,b) Low temperature deformation microfabrics within a syn-D_3 granitoid. (a) Weakly deformed alkali feldspar porphyroclast wrapped by a discrete mantle of fine-grained quartz and feldspar. Part of the feldspar that surrounds the porphyroclast may be the product of subgrain rotation recrystallisation. The arrow indicates a transgranular fracture. (b) Kinks of twinning planes in plagioclase. (c) Ultramylonitic micaschist of the Seridó Group in which quartz forms well-developed ribbons that define the Sm_3 foliation. (d) Oblique lamellae deformation (LD) and subgrain limits (SGL) demonstrate the effect of intracrystalline deformation within quartz grains of a syn-D_3 granitoid. (e) Evidence of pressure solution during the D_3 event in micaschist from the Seridó Group. The extreme attenuation of the vertical fold limb in the quartz veinlet coincides with dark seams along the S_3 foliation. (f) Later stage of the D_3 event in micaschist from de Seridó Group defined by greenschist facies dextral micro-shearbands (Sb), affecting the regional amphibolite facies D_3 mineral assemblage of biotite (Bt) + cordierite (Cd).

5. Microstructural investigation

Microstructural investigations were concentrated within D_2 and D_3 mylonitic fabrics. Distinctive aspects between these structures were obtained through feldspar and quartz microstructural investigations obtained from 200 thin-sections, oriented to contain both the normal to the foliations and the stretching lineations ($S_2/Sm_2-L_2^x$ and $S_3/Sm_3-L_2^x$). The analyzed thin-sections included the main lithotypes of the belt: granite-gneiss of the Caicó Complex, schists of the Seridó Group, syn-D_2 and syn-D_3 granitoids. Those samples oriented along D_2 fabrics were collected in regions where the flat lying S_2 foliation and N–S-trending L_2^x stretching lineation dominate (Fig. 4, domains 1, 2 and 4). To constrain estimates of temperature, deformation mechanisms and operation of slips systems, quartz *c*-axis measurements within pure quartz bands using conventional U-stage techniques and TEM investigations were performed.

5.1. D_2 microfabrics

Although mesoscopic evidence of D_2 deformation and kinematics is pervasively marked in all lithotypes of the belt, well-preserved feldspar and quartz microfabrics associated with this event were found principally within syn-D_2 granitoids and mylonitic gneisses of the Caicó Complex. In these rocks, feldspar and quartz are variably deformed by dynamic recrystallization that increases in intensity towards D_2 mylonite zones. In moderately deformed parts of D_2 shear zones, feldspar accommodates deformation by subgrain rotation recrystallization through the development of core-and-mantle structures in which undeformed or weakly deformed cores are typically surrounded by a narrow, partial to complete mantle of equant grains (Fig. 7a). Feldspar within D_2 shear zones, is extremely elongated parallel to the Sm_2 mylonitic foliation, defining the L_2^x stretching lineation. In these regions, most feldspars show evidence of grain boundary migration mechanisms, suggested by lobate and amoeboid contacts as well as the development of bulging structures (Fig. 7b and c). These structures progressively replace those formed by subgrain rotation recrystallization, indicating competition between the two mechanisms. Their simultaneous development in feldspar porphyroclasts is reported as evidence for high temperature deformation (regimes III of Hirth and Tullis (1992) and 'D' of Drury and Urai (1990)). Such competition is also recorded in quartz microfabrics, in which subgrain rotation is defined by core-and-mantle structures and grain polygonalization that culminates with bimodal banding. Evidence of grain boundary migration is observed along quartz-rich layers of syn-D_2 granitoids, with quartz forming mono- and polycrystalline ribbons strongly elongated along the Sm_2 mylonitic foliation (Fig. 7d). Bulging structures (Fig. 7e), dragging, serrate grain boundaries, and small strain-free grains are further evidence of grain boundary migration recrystallization. This behavior of quartz combined with ductile deformation of feldspar demands the imprinting of amphibolite facies conditions during formation of D_2 microfabrics. However, as such mechanisms were also operative under greenschist facies conditions, associated with the later stages of D_2, not only high temperatures should be invoked to explain the interplay of the subgrain rotation and grain boundary migration mechanisms, but also the dependence of their initial grain size. Then we state that the D_2 microfabrics might have been produced under near the equilibrium grain size in which the rate of new grain formation controlled by subgrain rotation recrystallization approximately matches the rate of grain consumption by grain boundary migration (Tullis, 1983; Bell and Johnson, 1989).

5.2. D_3 microfabrics

The most conspicuous characteristic of the D_3 event is the coexistence of high-T and low-T ductile fabrics (Vauchez et al., 1995). The first one represents the peak of metamorphic conditions, whereas low-T mylonites were formed late in the evolution of the belt. This coexistence could be misinterpreted in terms of overprinted deformational events if the structural elements, their geometry and kinematics have not indicated their progressive formation from deep crust, with pervasive ductile deformation, to shallow depths with development of narrow greenschist facies mylonite belts (Araújo et al., 2001).

The D_3 mylonitic zones contain a well-developed stretching lineation with intense deformation of quartz, biotite, muscovite and feldspars in the syn-D_3 granitoids and cordierite, andalusite and garnet in the metasediments. Quartz in these rocks shows strong undulatory extinction and dynamic recrystallization, with recrystallized grains associated with irregular patches and linear zones that surround porphyroclasts of feldspar. The latter does not show signs of ductile deformation, such as those observed along D_2 shear zones. Feldspar grains, however, deform principally by subgrain rotation, fracturing and pressure solution as illustrated in Fig. 8a. A few feldspar grains show limited intracrystalline deformation, demonstrated by the development of discrete undulatory extinction and kinks of twinning planes (Fig. 8b). Monocrystalline quartz ribbons (Fig. 8c) within ultramylonitic micaschists from the Seridó Group usually exhibit undulatory extinction and serrated grain boundaries. Quartz within less-strained rocks (protomylonites, particularly the syn-D_3 granitoids and micaschists) exhibits crude deformation bands, and lamellae deformation (Fig. 8d).

Participation of fluids during the D_3 event is indicated by the pervasive operation of pressure solution mechanisms.

Regionally, there is evidence for the presence of voluminous hydrous fluids infiltrated along the D_3 shear zones, which accounts for the extensive alteration of feldspar to fine grained aggregates of sericite, and partial to total conversion of biotite, cordierite and garnet to chlorite. The main microstructures related to pressure solution are truncated quartz grains, mica seams, attenuated limbs of F_3 microfolds and a well-developed dissolution banding (Fig. 8e). Some retrograde mineral transformations, such as chlorite, form continuous interconnected foliae that closely resemble recrystallized S–C mylonite textures, shear bands, and asymmetric micafish (Fig. 8f).

All the features described above suggest that D_3 mylonite zones continued to be active as the temperature decreased. This implies that D_3 shearing has been active for quite a long time during progressive down temperature deformation. Such a long period of ductile deformation is in agreement with 600–540 Ma zircon U–Pb and $^{40}Ar/^{39}Ar$ ages (Galindo et al., 1993; Corsini et al., 1998), which have been interpreted as the record of pervasive ductile deformation and cooling of these shear zones.

6. *c*-Axis fabrics and temperature conditions

Activation of slip systems of quartz is temperature sensitive. At low temperatures (lower-greenschist facies) and faster strain rates, for example, basal $\langle a \rangle$ slips induce the *c*-axis point maxima to concentrate near the *Z*-axis of the finite strain ellipsoid (Bouchez and Pêcher, 1981; Schmid and Casey, 1986). With increasing temperature (mid-greenschist facies), rhombohedral $\langle a \rangle$ slips become increasingly more important, forcing the *c*-axis maxima to migrate to intermediate positions between the *Y*- and *Z*-axes. At amphibolite conditions, the prism $\langle a \rangle$ slip system begins to be operative, resulting in point maxima near the *Y*-axis (Lister and Dornsiepen, 1982; Mainprice et al., 1986). Finally, at temperatures higher than 700 °C, prism $\langle c \rangle$ slip becomes active in quartz with *c*-axis concentrating near the *X*-axis (Mainprice et al., 1986). The switching from $\langle a \rangle$ to $\langle c \rangle$ slip systems usually occurs under temperatures higher than 700 °C, causing *c*-axis point maxima to migrate from near *Y*- to *X*-positions. However, similar *c*-axis fabrics have also been described in rocks that experienced temperatures

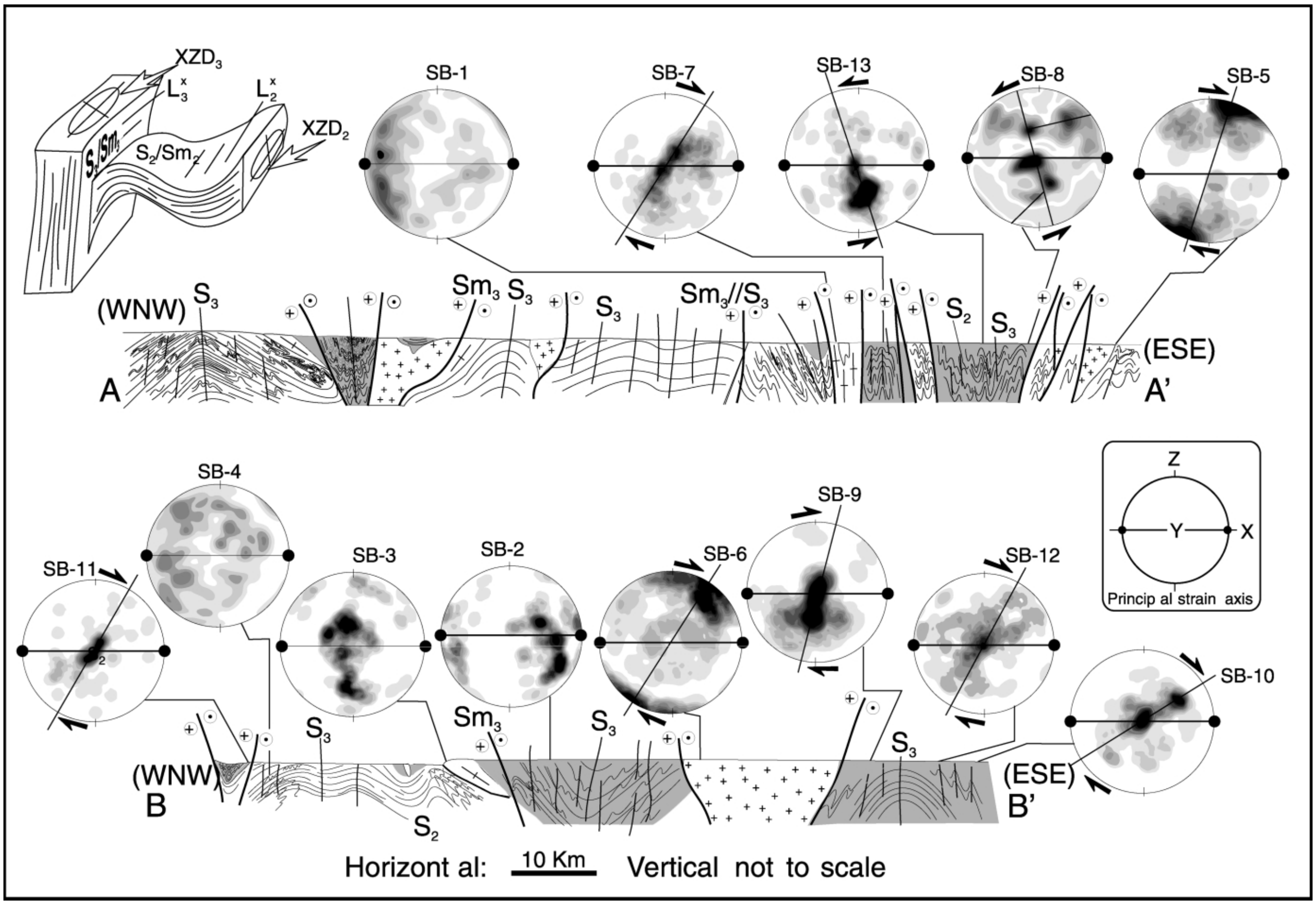

Fig. 9. Geological profiles (A–A′ and B–B′) cutting across the main structural trend of the Seridó Belt (location in Fig. 1). Quartz *c*-axis preferred orientations were measured in 13 samples collected along the profiles. *c*-Axis orientation is shown in the lower hemisphere of equal area projections with an average of 150 data contoured at 1–5 isolines. First isoline: uniform distribution, fifth isoline: maximum of 85%. As shown in the small inset at the right side of the illustration, *X* and *Y* represent the major and minor axis of the finite strain ellipsoid. The second inset at the upper left side is a schematic representation of the orientation of the *XZ* sections along D_2 and D_3 structures (XZD_2 and XZD_3, respectively). Samples SB-1–SB-4 were collected along D_2 structures, whereas the SB-5–SB-13 were collected along D_3 structures.

below 700 °C (Blumenfeld et al., 1986; Duebendrofer and Housten, 1987). High partial pressure of water, for example, is invoked to explain maxima near *X*- and *Y*-axes with operation of prism $\langle a \rangle$ and $\langle c \rangle$ systems being influenced either by reactive pore fluid (Smith and Evans, 1984) or by water weakening (Blacic, 1975; Mainprice et al., 1986). Finally, isolated maxima near *Y*-axis can also be produced by grain growth along the foliae of mica rich rocks (Hippertt, 1994). In this section, the configuration of quartz *c*-axis fabrics within D_2 and D_3 mylonites is used to help understand the thermal evolution of the Seridó Belt.

6.1. D_2 c-axis fabrics

c-Axis preferred orientations along the D_2 fabrics were measured from four samples collected distal to the strike-slip shear zones, in order to minimize the effect of the D_3 strain. The location of these samples is illustrated in Fig. 2. One hundred and fifty grains were measured from each thin-section. Quartz grains in contact with feldspar prophyroclasts were not measured to avoid contact strain effects (Lister and Price, 1978).

Quartz grains from D_2 mylonitic zones and their protoliths are xeno- to hypidiomorphic and strongly elongated parallel to the Sm_2 mylonitic foliation. Within mylonite gneisses and syn-D_2 granitoids, quartz grain sizes are in the range of 0.05–0.1 mm, whereas in micaschists within D_2 shear zones, this mineral is mainly xenomorphic with grain size in the range of 0.25–0.50 mm. In samples SB_1 and SB_2 (syn-D_2 granitoid and micaschist; see Fig. 9), at least two well-developed maxima near the stretching lineation (*X*-axis) were observed. This configuration could be attributed to activation of $\langle c \rangle$ prism slips triggered by high temperatures during deformation ($T > 700$ °C according to Garbut and Teyssier (1991)). Since thermal conditions in the Seridó Belt did not reach such high temperatures, other parameters than temperature must be invoked to interpret the operation of the $\langle c \rangle$ prism. In sample SB-1, a muscovite-sillimanite gneiss, near-*X* axis maxima, can be induced by preferential growth of quartz parallel to the mica foliae (according to Hippertt (1994)), which defines the S_2 foliation (Fig. 10). The same microstructural aspect is observed in sample SB-2, which is a micaschist that experienced amphibolite facies conditions. This behavior of quartz, combined with the abundance of fluid inclusion is here used to explain the near-*X* maxima from samples SB-1 and SB-2. Therefore, it can be assumed that the high content of phyllosilicate and high activity of intragranular H_2O caused the near-*X* *c*-axis fabrics during the high temperature stage of the D_2 event.

The third sample (SB-3), a syn-D_2 granitoid, showed basically single girdle *c*-axis distribution with remnants of type I crossed girdle (Lister, 1977). In this sample, maxima occur at intermediate positions in relation to the *Z*- and *Y*-axes (profile B–B′; Fig. 9). The *c*-axis pattern exhibited in sample SB-3 shows well-developed point maxima occupying positions correlative to site III of Fueten (1992), which may result from retrogressive metamorphism associated operative positive and negatives $\langle a \rangle$ rhombs, during later stages of D_3-shearing. Textural evidence of feldspars and biotite being transformed into white mica and chlorite, respectively, confirms the operation of retrogressive transformations in the sample SB-3 (Fig. 3d). Finally, one sample from a Caicó Complex orthogneiss (SB-4) shows a poorly developed *c*-axis preferred orientation, in which the maxima appear scattered in the diagram. As the rocks from the Caicó Complex experienced deformation during an older event (D_1), the poorly developed *c*-axis pattern of sample SB-4 may be the result of its partial obliteration owing to the overprinting of the D_2 event.

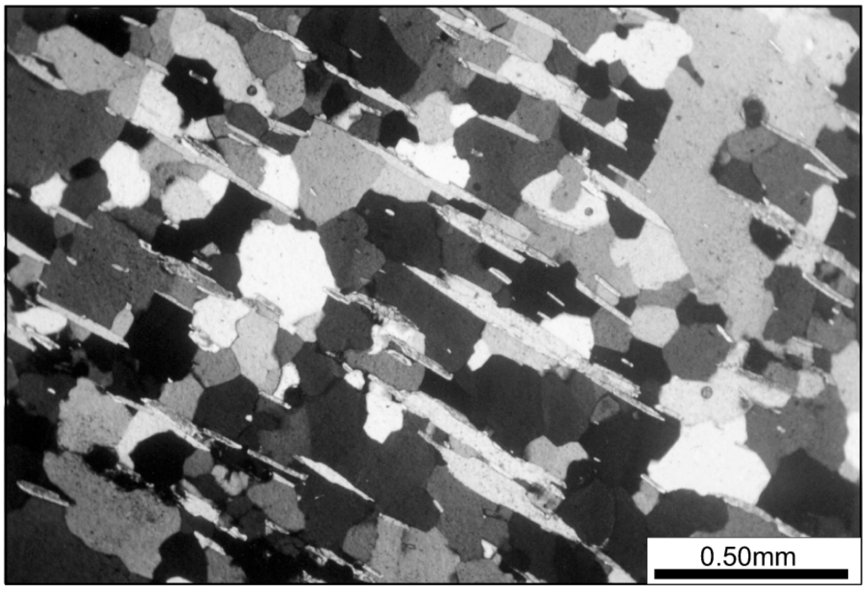

Fig. 10. Preferential growth of quartz grains following the mica foliae within granite gneiss of the Caicó Complex.

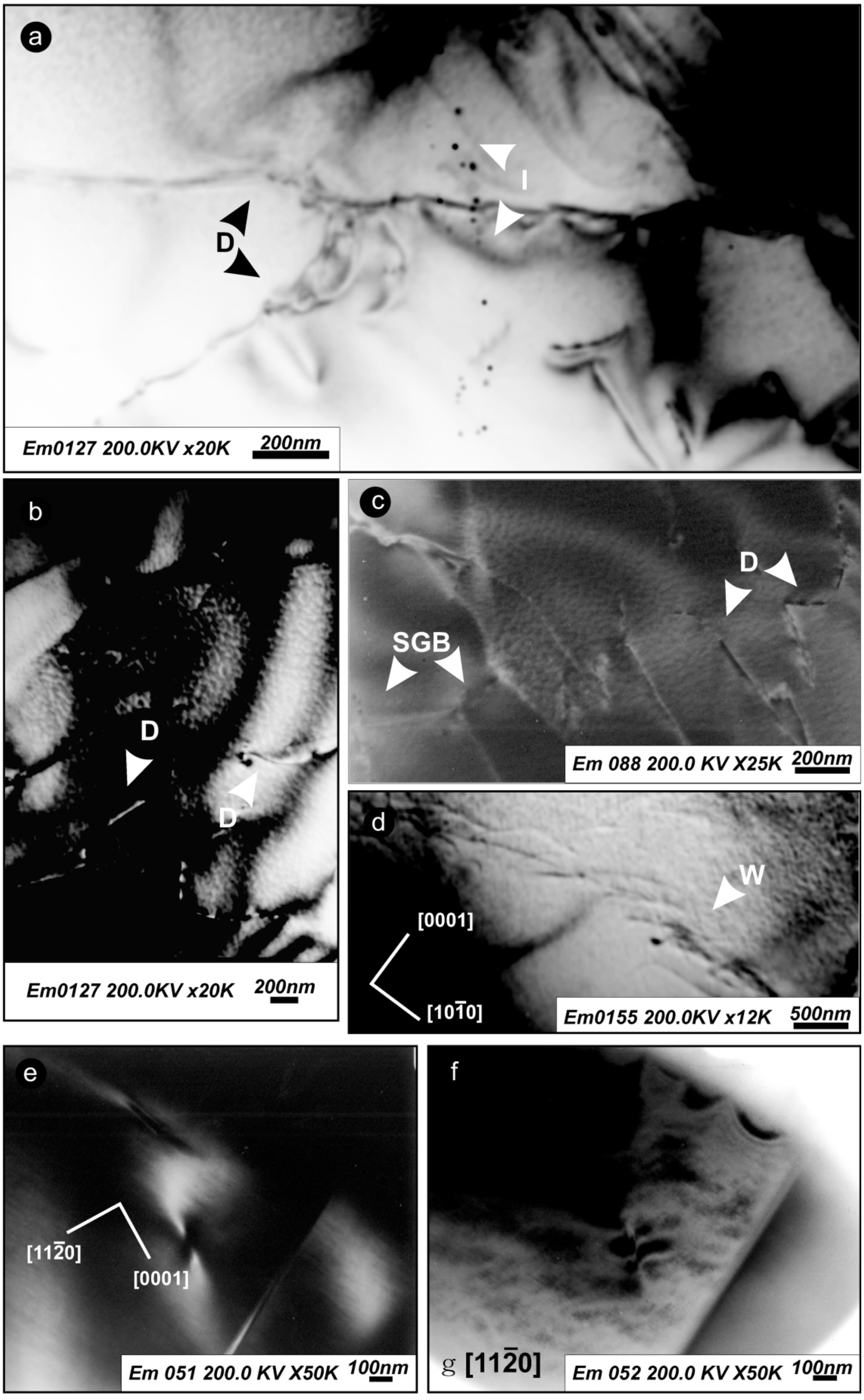
a
I
D
Em0127 200.0KV x20K 200nm
b
D
D
Em0127 200.0KV x20K 200nm
c
D
SGB
Em 088 200.0 KV X25K 200nm
d
W
[0001]
[10$\bar{1}$0]
Em0155 200.0KV x12K 500nm
e
[11$\bar{2}$0]
[0001]
Em 051 200.0 KV X50K 100nm
f
g [11$\bar{2}$0]
Em 052 200.0 KV X50K 100nm

6.2. D_3 c-axis fabrics

Quartz *c*-axis measurements of D_3 microfabrics were obtained from nine samples collected along the A–A′ and B–B′ profiles illustrated in Fig. 9. The SB-5 and SB-6 samples were collected within mylonite zones affecting the boundaries of syn-D_3 granitoids, whereas the other seven (SB-7–SB-13) are from mylonite schists of the Seridó Group. In these rocks, quartz grains ranging from 0.5 to1.0 mm can occur either in association with the other constituents of the matrix (feldspars, phyllosilicates, etc.) or by forming enriched bands interlayered with micaceous bands. Within the syn-D_3 granitoids, quartz dominates the fine-grained matrix (0.05–0.1 mm), which includes minor amounts of biotite, muscovite, chlorite, apatite, epidote and titanite.

Contrasting with the D_2 *c*-axis determinations, external asymmetry of *c*-axis fabrics from D_3 shear zones can be used as a kinematic indicator. Well-developed type I crossed girdles in samples SB-5 and SB-6 show the maxima asymmetrically distributed in relation to the *Z*-axis. This, in conjunction with the configuration of maxima and the submaxima in samples SB-7, SB-9, SB-11, and SB-12 confirms the dextral shear sense obtained with meso- and microscopic kinematic indicators. Samples SB-8 and SB-13 (profile A–A′; Fig. 9), however, indicate a sinistral sense of shearing that contrasts with the bulk dextral kinematics of the D_3 event. This opposite kinematics could be attributed to localized reverse shearing (general shear $0 \leq \mathrm{Wk} \leq 1$) as a result of the transpressive kinematics that dominates the central portion of the Seridó Belt. Similar inversions have been documented elsewhere at transpressive belts (Hippertt and Tohver, 1999; Wolfgan and Kurz, 2000).

With regard to their internal geometry, quartz *c*-axis fabrics from D_3 microfabrics are mostly characterized by maxima near the *Y*-axis (Fig. 9). This situation could result from deformation under amphibolite facies conditions. However, a similar *c*-axis pattern is also present within rocks that experienced mylonitization under greenschist facies conditions as indicated by paragenesis quartz + chlorite + biotite. Here, we suggest that development of a near-*Y* maximum, as illustrated in Fig. 9 (samples SB-7, 8, and 10–13), was caused by activation of the $\langle a \rangle$ prism slip system controlled by parameters other than uniquely higher temperatures, particularly when *c*-axis fabrics from greenschist facies mylonites are taken into account. The pervasive development of pressure solution along the D_3 shear zones reveals a strong influence of fluids during the evolution of these mylonite zones. These fluids may have exerted an important effect on the operation of the $\langle a \rangle$ prism system. On the other hand, *Y*-maximum was also observed in rocks away from the D_3 shear zones, in which pressure solution microstructures were not recognized. In this case, the operation of $\langle a \rangle$ prism slips may have resulted from deformation under amphibolite facies conditions with minor influence of fluids. At first glance, this seems to be an ambiguous situation; nonetheless, it can be explained by the competition of thermally and fluid activated $\langle a \rangle$ prism slip systems from the outward to the inward parts of the D_3 shear zones. This would favor the activation of $\langle a \rangle$ prism slips within greenschist facies D_3 shear zones, in which fluid channeling along the Sm_3 mylonitic fabric favored weakening of quartz.

A second configuration of *c*-axis is delineated by equally well-developed *Z*-maxima or submaxima at intermediate position between the *Y*- and *Z*-axes. In samples SB-5 and SB-6, quartz *c*-axis fabrics obtained from greenschist facies mylonite zones affecting boundaries of two different syn-D_3 plutons (Fig. 9), show as densely populated near the *Z*-axis. These patterns suggest activation of the $\langle a \rangle$ basal slip, which is the glide system of quartz with lower activation energy at low metamorphic grade conditions (Fueten, 1992). The second case, in which the *c*-axis fabrics show submaxima at an intermediate position between *Y* and *Z* (samples SB-8 and SB-10 in Fig. 9), agrees with the evolution of the belt from deeper to shallower crustal levels, as a result of decreasing temperatures. Quartz *c*-axis fabrics observed in these two samples are associated here with switching from $\langle a \rangle$ prism to $\langle a \rangle$ basal slips during cooling and continued shearing along D_3 shear zones.

7. TEM investigations

TEM investigation along the studied microfabrics was conducted to determine dislocation patterns and slip systems operative in quartz during the superposed D_2 and D_3 events. To confirm our understanding of the operative slip systems TEM observations were made within quartz grains from syn-D_2 and syn-D_3 granitoids (samples SB-1–SB-6 in the A–A′ and B–B′ profiles shown in Fig. 9). Following optical studies, individual quartz grains containing well-defined subgrain boundaries were selected. The samples were thinned and carbon coated, being analyzed with a 200 kV JEOL JEM2010FX at the Centre of Microscopy and Microanalyses of the University of Queensland, Australia.

7.1. Dislocation patterns

At a submicroscopic scale, quartz from both samples exhibit free dislocations with straight or curved boundaries

Fig. 11. (a) Bright field image showing free dislocations (D) within quartz from a G_2 granitoid (sample SB-1). The arrows indicate small inclusions (I), no larger than 10 nm, with ovoid shape and negative contrast. (b) Free dislocations with straight or curved boundaries in sample SB-1. (c) Dislocations and subgrain boundaries (SGB) oriented normal to the foliation plane of a G_3 granitoid (sample SB-5). (d) Dislocation walls (W) nearly parallel to *c* [0001] plane. (e) Bright field image of a free dislocation parallel to [0001]. (f) Dark field image from the same area. Diffraction vector $\mathbf{g} = [11\bar{2}0]$.

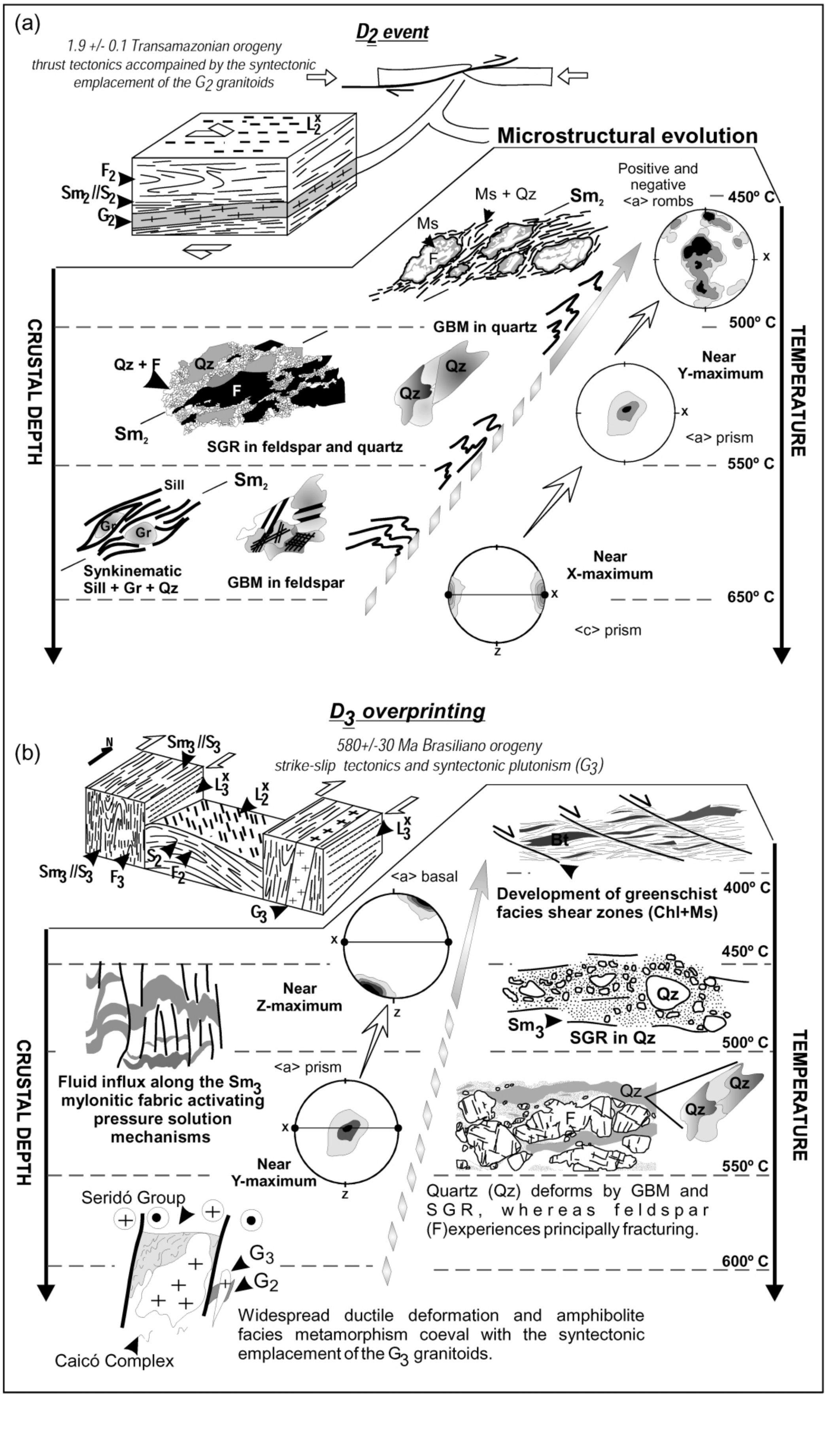

(a)
D2 event
1.9 +/- 0.1 Transamazonian orogeny
thrust tectonics accompanied by the syntectonic
emplacement of the G2 granitoids
Microstructural evolution
Positive and negative <a> rombs
450º C
500º C
550º C
650º C
GBM in quartz
Near Y-maximum
<a> prism
Near X-maximum
<c> prism
SGR in feldspar and quartz
Synkinematic Sill + Gr + Qz
GBM in feldspar
CRUSTAL DEPTH
TEMPERATURE
D3 overprinting
(b)
580+/-30 Ma Brasiliano orogeny
strike-slip tectonics and syntectonic plutonism (G3)
<a> basal
Development of greenschist facies shear zones (Chl+Ms)
400º C
450º C
500º C
550º C
600º C
Near Z-maximum
SGR in Qz
<a> prism
Fluid influx along the Sm3 mylonitic fabric activating pressure solution mechanisms
Near Y-maximum
Quartz (Qz) deforms by GBM and SGR, whereas feldspar (F)experiences principally fracturing.
Seridó Group
Caicó Complex
Widespread ductile deformation and amphibolite facies metamorphism coeval with the syntectonic emplacement of the G3 granitoids.

(Fig.11a and b). In sample SB-1, however, these dislocations are decorated with small inclusions (≈10 nm; Fig. 11a) that display ovoid to negative crystal shapes and show contrast consistent with that expected from fluid bubbles (McLaren, 1991). This feature is in agreement with the microstructural verifications and confirms that fluid, at some extent, participated during the D_2 event. In sample SB-6, on the other hand, this feature is not well-developed and large quartz grains (typically >200 nm) are dominated by subgrain boundaries and dislocation arrays preferentially aligned either parallel or perpendicular to the foliation (Fig. 11c). In this sample, most of the subgrain dislocation walls either define boundaries or networks (Fig. 11c and d) nearly normal to [0001]. This corroborates the interpretation of $\langle a \rangle$ basal slips estimated based on quartz *c*-axis fabrics.

From the above, it can be considered that the dislocation glide was an important crystal-plastic deformation mechanism during both D_2 and D_3 events; however, it operated differently during the formation of each microfabric set.

7.2. Operative slip systems

Although participation of fluids favoring the operation of $\langle c \rangle$ prism slip system during D_2 has been confirmed at micro- and submicroscopic scale fluid inclusions, an analysis of operative slip systems in quartz from one syn-D_2 granitoid using the standard technique of 'invisibility criteria' was also undertaken (McLaren, 1991 and references therein). For a dislocation to be invisible, the following condition is required: the vector products $\mathbf{g}\cdot\mathbf{b} = 0$ for pure screw dislocation, and $\mathbf{g}\cdot\mathbf{b} \times \mathbf{u} = 0$ for edge dislocation, where $\mathbf{g}$ is the diffracting vector, $\mathbf{b}$ the Burgers vector and $\mathbf{u}$ the unit vector along the dislocation line.

Bright and dark field images of a free dislocation in quartz from sample SB-1 are shown in Fig. 11e and f, respectively. Since the dislocation is almost out of contrast in the dark field image using the diffraction $\mathbf{g} = [11\bar{2}0]$, and owing to its being nearly parallel to [0001], the dislocation must be identified as a screw dislocation with a Burgers vector of [0001]. This observation combined with near-X *c*-axis maxima in samples SB_1, SB_2 and SB_3 is consistent with activation of $\langle c \rangle$ prism slips during the D_2 event.

8. Tectono-thermal evolution of the Seridó belt: discussions and conclusions

Results of this study suggest that microstructures and *c*-axis fabrics in quartz of rocks from polydeformed terrains can record successive thermal episodes. In the Seridó Belt the compatibility of thermal conditions in mineral assemblages and *c*-axis fabrics in quartz demonstrates the reliability of the latter and preserve the record of early tectonothermal events. Besides improving the knowledge of the Seridó Belt, such contributions can also help the understanding of overprinting thermal episodes in other orogenic belts. Particularly in the African counterpart of the Borborema Province (e.g. Trans-Saharan belt), in which the Brasiliano/Pan-African (600 Ma) event reworks crustal blocks deformed during the Eburnean Event at 2.0 Ga (Boullier, 1991).

In this work, preserved microstructures and quartz *c*-axis fabrics related to D_2 and D_3 are unlikely to be integrated into a single progressive P–T–t–d path (Fig. 12). Microfabrics and quartz *c*-axis fabrics from 1.9 Ga granitoids and their host rocks coupled with synkinematic formation of kyanite + sillimanite + garnet along D_2 shear zones, demonstrates that temperatures around 600–650 °C were reached during the metamorphic peak of the D_2 event. These temperatures and intragranular fluids worked together favoring the operation of $\langle c \rangle$ prism slips, defined by *c*-axis maxima near or at an intermediate position in relation to the *X*-axis, TEM observations of (0001) subgrain boundaries and free dislocations with [0001] Burgers vector. Retrogressive transformations of biotite and feldspars along the Sm_2 mylonitic foliation and *c*-axis maxima in positions correlative to the site III of Fueten (1992) demonstrates the temperature decrease at the later stages of D_2. Such a thermal path is compatible with the interpretation of D_2 as a thrust event, with shearing and widespread ductile deformation at high crustal depths, and low-temperature modifications of the quartz *c*-axis fabrics (see Fig. 12a) produced by further motion of the thrust sheet, uplift and cooling of the terrain.

During D_3 the region underwent pervasive ductile deformation coeval with the Brasiliano strike-slip event and granitic magmatism (600 Ma; see Fig. 12b). Thermal conditions of 600 °C within micaschists of the Seridó Group were associated with the peak of deformation and metamorphism during this event. Similar temperatures have been found at Neoproterozoic segments of the Borborema Province, in which widespread mylonitization and metamorphism reached 600–650 °C (Neves et al., 2000). Although these temperatures are similar to those determined for the D_2 event, the presence of relicts of syn-D_2 kyanite + sillimanite, partially replaced by muscovite, as inclusions within the syn-D_3 andalusite and cordierite porphyroblasts demonstrate that the Seridó belt experienced a second thermal event. The analysis of microfabrics and quartz *c*-axis fabrics along the D_3 shear zones that overprint D_2 fabrics, confirms this superposition.

Fig. 12. Cartoon showing the tectonothermal evolution of the Seridó Belt during (a) D_2 and (b) D_3 events. Thermal paths during these events are demonstrated with a basis on microstructures and *c*-axis patterns in quartz. (GBM) grain boundary migration, (SGR) subgrain rotation, (Ms) muscovite, (Chl) chlorite.

The coexistence of low-T and high-T mylonite belts, deformation mechanisms and *c*-axis fabrics combined with U–Pb ages and ^{40}Ar–^{39}Ar ages in the interval of 600†540 Ma supports the interpretation that the D_3 ductile deformation was active for a long term in the Seridó Belt. During this long period, mylonite zones experienced a large variety of deformation mechanisms, likely to be formed at different thermal increments of the D_3 event (see Fig. 12b). Here, the plastic behavior of quartz grains, texturally illustrated by the development of interlobate grain boundaries and ribbons, are implicated in the mechanism of dislocation creep and glide are documented. Feldspars, however, are typically fractured or undeformed and wrapped by the Sm_3 foliation that is pronounced within the quartz rich layers. These microstructures are coeval with temperatures of 350 ± 50 °C, being compatible with the activation of $\langle a \rangle$ basal slips in quartz during the later stages of the D_3 event.

In the middle of the D_3 shear zones, the participation of fluids was absolutely fundamental to the generation of the Sm_3 mylonitic fabric. Within these zones the influence of fluid during the D_3 event was more pervasive, as shown by the extensive replacement of dynamic recrystallization for pressure solution microstructures. This deformation mechanism has been also marked in quartz *c*-axis fabrics that show near-Y maxima, being attributed to the accommodation of intracrystalline deformation by $\langle a \rangle$ prismatic slips activated under intermediate to low temperatures and fluid abundance.

Therefore, it can be concluded that besides having overprinted the D_2 fabrics, the D_3 event also evolved from high to low temperatures simultaneously with the exhumation and cooling of the terrain. This implies subsequent thermal overprint, which had direct influence on the quartz *c*-axis fabrics along D_3 shear zones. Hence, the thermal evolution of the Seridó belt, according to the evidence presented in this paper, developed through two distinct tectono-thermal events, being recorded not only by incompatibility of mineral assemblages, but also principally by thermally and fluid activated slip systems and deformation mechanisms. The difficulty of integrating D_2 and D_3 tectono-thermal events in a single P–t–t–d path supports the interpretation of a polyphase evolution for the Belt. Neoproterozoic ages for the Seridó Group, however, are still questionable in terms of its regional extent and significance. On the other hand, these young ages are not totally ruled out, since part of the Seridó Group could have been deposited during this time, as proposed by Archanjo and Salim (1986). Based on all these aspects, it is believed that nearly all the Seridó Belt experienced two tectono-thermal events, a 1.9 Ga south-directed thrust tectonics and a second event of crustal reworking with pervasive ductile deformation at 600 Ma, evolving lately through the development of low-T shear zones at 540 Ma.

Acknowledgements

This present paper is an outcome of the doctoral research on Precambrian rocks in the Northeast of Brazil carried out by M. Araújo. Financial support for this work was provided by the Brazilian National Research Council (CNPq, process 200504/00-2) and by the PADCTIII/FINEP project "Controle Estrutural e Geocronológico das Mineralizações de Au e W nas Faixas Seridó e Cachoeirinha". We are grateful to the Department of Earth Sciences of the University of Queensland/Australia, where M.N.C.A. carried out quartz *c*-axis measurements and TEM investigations. We would also like to thank Elson Paiva de Oliveira (Institute of Geosciences of the UNICAMP, Brazil) for the constructive comments and for improving the English. Reviews by M. Egydio-Silva and K. Hickey considerably improved the manuscript.

References

Affaton, P., Rahaman, M.A., Trompette, R., Sougy, J., 1991. The Dahomeyde orogen: tectonothermal evolution and relationships with the Volta basin. In: Dallmeyer, R.D., Lércorché, J.P. (Eds.), The West African Orogens and Their Circum-Atlantic Correlatives, Springer-Verlag, Berlin, pp. 101–122.

Araújo, M.N.C., Alves da Silva, F.C., Jardim de Sa, E.F., 2001. Pegmatite emplacement in the Seridó Belt, Northeastern Brazil: late stage kinematics of the Brasiliano Orogen. Gondwana Research 1, 75–85.

Archanjo, C.J., Bouchez, J.L., 1991. Le Seridó, une chaine transpressive dextre au Protérozoique supérieur du Nord-Est du Brésil. Bulletin de la Societé Geologique de France 162, 637–647.

Archanjo, C.J., Salim, J., 1986. Posição da Formação Seridó no contexto estratigráfico regional (RN-PB). SBG Abstracts, Simpósio de Geologia do Nordeste 12, 270–281.

Bell, T.H., Johnson, S.E., 1989. The role of deformation partitioning in the deformation and recrystallization of plagioclase and K-feldspar in the Woodroffe thrust zone, central Australia. Journal of Metamorphic Geology 7, 151–168.

Bertrand, J.M., Jardim de Sá, E.F., 1990. Where are the Eburnean-Transamazonian Collisional Belts? Canadian Journal of Earth Sciences 27; 1382–1393.

Blacic, J.D., 1975. Plastic deformation mechanisms in quartz the effect of water. Tectonophysics 2, 171–194.

Blumenfeld, P., Bouchez, J.L., Mainprice, D., 1986. C-slip in quartz from subsolidus deformed granite. Tectonophysics 127, 97–115.

Bouchez, J.L., Pêcher, A., 1981. The Himalayan main central thrust pile and its quartz-rich tectonites in Central Nepal. Tectonophysics 78, 23–50.

Boullier, A.M., 1991. The Pan-African Trans-Saharan Belt in the Hoggar Shield (Algeria, Mali, Niger): a review. In: Dallmeyer, R.D., Lércorché, J.P. (Eds.), The West African Orogens and Their Circum-Atlantic Correlatives, Springer-Verlag, Berlin, pp. 85–105.

Caby, R., Arthaud, M., Archanjo, C.J., 1995. Lithostratigraphy and petrostructural characterisation of supracrustal units in the Brasiliano Belt of Northeast Brazil: geodynamic implications. Journal of South American Earth Sciences 8, 235–246.

Corsini, M., Figueiredo, L.L., Caby, R., Féraud, G., Ruffet, G., Vauchez, A., 1998. Thermal history of the Pan-African/Brasiliano Borborema Province of northeast Brazil deduced from $^{40}Ar/^{39}Ar$ analysis. Tectonophysics 285, 103–117.

Dantas, E., Van Schmus, W.R., Hackspacher, P.C., Fetter, A., Brito Neves, B.B., 1999. Identification of multiple orogenic/metamorphic events in polycyclic terranes; possibilities and limitations. Insights from the

Borborema Province, NE Brazil. Abstracts, International Symposium in Tectonics of the SBG, Lençois, Bahia, Brazil 1, pp. 15–17.

Drury, M.R., Urai, J.L., 1990. Deformation-related recrystallization processes. Tectonophysics 172, 235–253.

Duebendrofer, E.M., Housten, R.S., 1987. Proterozoic accrectionary tectonics at the southern margin of the Archean Wyoming craton. Geological Society of America Bulletin 98, 554–568.

Fonseca, V.P., Barbalho, A.H.P., Jardim de Sá, E.F., 1991. Metamorfismo barroviano na Faixa Seridó e seu contexto tectônico: caso da região de Lages (RN). SBG Abstracts, Simpósio de Geologia do Nordeste 14 (1), 240–243.

Fueten, F., 1992. Tectonic interpretations of systematic variations in quartz *c*-axis fabrics across the Thompsom Belt. Journal of Structural Geology 14, 775–789.

Galindo, A.C., Dall'Agnol, R., McReath, I., Sheller, T., 1993. Geocronologia dos granitóides brasilianos da região de Caraúbas-Umarizal, Oeste do Rio Grande do Norte. SBG Abstracts, Simpósio de Geologia do Nordeste, Recife 1, 325–328.

Garbut, J.M., Teyssier, C., 1991. Prism $\langle c \rangle$ slip in quartzites of the Okhurst mylonite belt, California. Journal of Structural Geology 13, 657–666.

Gleason, G.C., Tullis, J., Heidelbach, F., 1993. The role of dynamic recrystallization in the development of lattice preferred orientations in experimentally deformed quartz aggregates. Journal of Structural Geology 15, 1145–1168.

Hippertt, J.F., 1994. Microstructures and *c*-axis fabrics indicative of quartz dissolution in sheared quartzites and phyllonites. Tectonophysics 229, 141–163.

Hippertt, J.F., Tohver, E., 1999. On the development of zones of reverse shearing in mylonitic rocks. Journal of Structural Geology 21, 1603–1614.

Hirth, G., Tullis, J., 1992. Dislocation creep regimes in quartz aggregates. Journal of Structural Geology 14, 145–159.

Jardim de Sá, E.F., Macedo, M.H.F., Pecaut, J.J., Kawashita, K., Souza, Z.S., Bertrand, J.M., 1995. Pré-brasiliano orogenic evolution in the Seridó Belt, NE Brazil: conflicting geochronological and structural data. Revista Brasileira de Geociências 25, 107–146.

Jardim de Sá, E.F., Trindade, R.I.F., Hollanda, M.H.B.M., Araújo, J.M.M., Galindo, A.C., Amaro, V.E., Souza, Z.S., Vigneresse, J.L., Lardeaux, J.M., 1999. Brasiliano syntectonic granites emplaced in a strike slip/extensional setting (eastern Seridó Belt, NE Brazil). Anais da Academia Brasileira de Ciências 71, 17–27.

Jessel, M.W., Lister, G.S., 1990. A simulation of the temperature dependence of quartz fabrics. In: Knipe, R.J., Rutter, E.H. (Eds.), Deformation Mechanisms, Rheology and Tectonics. Geological Society Special Publication 54, pp. 353–362.

Kozuch, M., Van Schmus, W.R., Brito Neves, B.B., 1997. Ages and isotope geochemistry of two pre-brasiliano magmatic events in the Borborema Province of NE Brazil. South American Symposium on Isotope Geology, Abstracts, 157–160.

Legrand, J.M., França, V.M.Q., 1989. Implicação geotectônica do metamorfismo brasiliano da Faixa Seridó (RN) e suas relações com os granitóides intrusivos. SBG Abstracts, Simpósio Nacional de Estudos Tectônicos 2, 233–236.

Leterrier, J., Jardim de Sá, E.F., Bertrand, J.M., Pin, C., 1994. Ages U–Pb sur zircon de granitoides "brasiliano" de la ceinture do Seridó (Province Borborema, NE Brésil). Comptes Rendus de l'Académie des Science de Paris II 318, 1505–1511.

Lister, G.S., 1977. Crossed girdle *c*-axis fabrics in quartzites plastically deformed by plane strain and progressive simple shear. Tectonophysics 39, 51–54.

Lister, G.S., Dornsiepen, U.L., 1982. Fabric transitions in the Saxony granulite terrane. Journal of Structural Geology 4, 81–92.

Lister, G.S., Price, G.P., 1978. Fabric development in a quartz feldspar mylonite. Tectonophysics 49, 37–78.

McLaren, A.C., 1991. Transmission Electron Microscopy of Minerals and Rocks, Cambridge University Press, Cambridge.

Mainprice, D., Bouchez, J.L., Blumenfeld, P., Tubia, J.M., 1986. Dominant c slip in naturally deformed quartz: implications for dramatic plastic softening at high temperature. Geology 14, 819–822.

Mazurek, M., 1992. Phase-equilibria and oxygen isotopes in the evolution of metapelitic migmatites—a case-study from the pre-alpine basement of Northern Switzerland. Contributions to Mineralogy and Petrology 109, 494–510.

Neves, S.P., Vauchez, A., Feraud, G., 2000. Tectono-thermal evolution, magma emplacement and shear zone development in the Caruaru area (Borborema Province, NE Brazil). Precambrian Research 99, 1–32.

Passchier, C.W., Trouw, R.A.J., 1996. Microtectonics, Springer-Verlag, Berlin.

Ralser, S., 2000. Microstructural constraints on timing of Proterozoic deformation in Central New Mexico. Journal of Metamorphic Geology 18, 457–466.

Ramsay, J.G., Hubber, M.I., 1987. The Techniques of Modern Structural Geology and Strain Analysis, Academic Press, London.

Schmid, S.M., Casey, M., 1986. Complete fabric analysis of some commonly observed quartz *c*-axis patterns. In: Hobbs, B.E., Heard, H.C. (Eds.), Mineral and Rocks Deformation: Laboratory Studies—The Patterson Volume. American Geophysicists Union, Geophysical Monograph 36, pp. 263–286.

Smith, D.L., Evans, B., 1984. Diffusional crack healing in quartz. Journal of Geophysical Research 89, 4125–4136.

Souza, L.C., 1996. Zoneographie metamorphique, chimie des mineraux, petrochimie, geochronologie $^{40}Ar/^{39}Ar$ et histoire P–T–t des micaschistes englobant le massif gabro-granitique d'Acari (Brasiliano), Ceinture Moblile du Seridó (NE du Bresil). Unpublished PhD Thesis, Université de Louvain.

Tullis, J., 1983. Deformation of feldspars. In: Ribbe, P.H., (Ed.), Feldspar Mineralogy, Mineralogical Society of America, pp. 297–323.

Van Schmus, W.R., Brito Neves, B.B., Williams, I.S., Fetter, A.H., Hackspacher, P.C., 2000. The Seridó Group, NE Brazil: a Late Neoproterozoic (650 Ma), pre-collisional, Brasiliano Flysch Basin? SBG, International Geological Congress, 31, Rio de Janeiro, Brazil, CD-Rom.

Vauchez, A., Neves, S., Caby, R., Corsini, M., Egydio-Silva, M., Arthaud, M., Amaro, V., 1995. The Borborema shear zone system, NE Brazil. Journal of South American Earth Sciences 8, 247–266.

White, J.C., Mawer, C.K., 1992. Deep-crustal deformation textures along megathrusts from Newfoundland and Ontario: implications for microstructural preservation, strain rates, and strength of the lithosphere. Canadian Journal of Earth Sciences 29, 328–337.

Wolfgan, U., Kurz, W., 2000. Progressive development of lattice preferred orientation (LPOs) of naturally deformed quartz within a transpressional collision zone (Panafrican Orogen in the Eastern Desert of Egypt). Journal of Structural Geology 22, 1827–1835.

Yardley, B.W.D., 1989. An Introduction to Metamorphic Petrology, Logman Group UK Ltd, London.